Modeling Spontaneous Charge Transfer at Metal/Organic Hybrid Heterostructures

V. Ongun Özçelik,*,†,‡ Yingmin Li,*,‡ Wei Xiong,*,†,‡ and Francesco Paesani*,†,‡,¶

†Department of Chemistry and Biochemistry, University of California San Diego, La Jolla, CA 92093 United States.

‡Materials Science and Engineering Program, University of California San Diego, La Jolla, CA 92093 United States.

¶San Diego Supercomputer Center, University of California San Diego, La Jolla, CA
92093 United States.

E-mail: vozcelik@ucsd.edu; yil233@eng.ucsd.edu; w2xiong@ucsd.edu; fpaesani@ucsd.edu

Abstract

Hybrid heterostructures are crucial in photovoltaics where the overall efficiency of the materials are closely related to the level of charge transfer at their interfaces. Here, using a combined computational and experimental approach, we show that heterodyne vibrational sum frequency generation (HD-VSFG) measurements provide an effective way of monitoring the interfacial charge transfer in these heterostructures. Using abinitio quantum chemical calculations, we show that inducing regio-randomness into the organic polymer modifies the interfacial electronic states, level of hybridization and the electronic wave function of these materials. We present the HD-VSFG responses of the metal/P3HT heterojunctions containing both regio-regular and regio-random P3HT structures and show that the intensity of non-resonant signal is directly correlated with the computed electronic structure and the level of spontaneous charge transfer at these interfaces.

Integration of surfaces with ultra thin materials is essential for designing hybrid functional devices where the unique functionalities arising at their interface strongly influence the overall properties of the heterostructure beyond those of the isolated materials. In this regard, the development of hybrid heterostructures comprising an inorganic substrate and a thin film of organic polymer is a recent milestone achieved in molecular electronics, battery electrodes and photovoltaics research. 2-5 Upon creating a physical contact between a polymer and a metallic substrate, charge separation can happen in the heterostructure where the hole states are localized in the organic polymer and the electrons transfer into the substrate, which we refer herein as spontaneous charge transfer. Spontaneous charge transfer plays a crucial role in defining the optical and electronic efficiencies of the heterostructure since the charge accumulated around the contact region influences the interfacial electronic structure and coupling.⁶ This process depends on the atomic structure of the junction, the chemistry of the substrate and the organic polymer, conformation of the polymer on the substrate and the level of hybridization between the substrate and the polymer. 7,8 Thus, a precise fundamental understanding of these properties and their effect on the spontaneous charge transfer mechanism is the first step toward the molecular engineering of metal / organic interfaces which will be used in macroscopic assembly of solid state structures for molecular electronics and conductive coating for battery electrodes.

Despite its significance, spontaneous charge transfer in hybrid heterostructures is difficult to monitor with surface scanning techniques such as scanning tunneling microscopy or atomic force microscopy due to the fact that electron transfer interfaces are hidden by the bulk materials. 9,10 Photoelectron spectroscopy can be used to extract the band structure at interfaces, however it is still limited to thin film interfaces due to the short penetration depth of photoelectrons. 11 Additionally, up until now there has been no direct study investigating the connection between the regio-randomness of the polymer and the charge transfer properties of hybrid interfaces. Here, we address this fundamentally significant problem using a hybrid experiment-theory approach to probe interfacial electronic structure reorganization

of complex interfaces. We show that HD-VSFG technique provides an effective way for monitoring the level of spontaneous charge transfer in metal/organic hybrid structures. This is of broad significance for flexible electronics, optoelectronics and photocatalysis communities since controlling the level of charge transfer in metal/organic interfaces is crucial for the material's efficiency.

In hybrid photovoltaic materials, using P3HT as the conjugated organic polymer is common due to its high solubility, environmental stability and high electron mobility. 4,12–15 Therefore, here we focus on various P3HT samples deposited on metal substrates and using ab-initio quantum chemical calculations based on density functional theory (DFT) we reveal that (i) the level of charge transfer and electronic coupling at the interface can be selectively engineered by controlling the conformational regularity of the organic polymer, (ii) the geometrical regio-randomness of the organic polymer not only changes the charge transfer between the layers but it also determines how interlayer states arise at the interface, and (iii) these interlayer states significantly modify the level of hybridization, surface carrier density, local electrostatic potential and the wave function of the material. We compare our calculated charge transfer results with the experimentally obtained non-resonant and resonant responses of the HD-VSFG signals for these materials. We show that the amount of non-resonant signal is directly correlated with the computed level of charge transfer at the interface. Our results justify that HD-VSFG signal can be used as an indicator for probing spontaneous interfacial charge transfer and demonstrate that the spontaneous charge transfer between P3HT and metal substrate significantly depends on the regio-regularity of the polymer.

The computed geometry of an isolated P3HT molecule is presented in Figure 1(a), where the monomer consists of a π -conjugated thiophene backbone and two alkyl side chains. P3HT monomers can be arranged in a sequential order to construct various types of P3HT polymer chains which differ by how the side chains are located in alternating monomers as shown Figure 1(b-c). Accordingly, these polymers can be divided into two subgroups: (i)

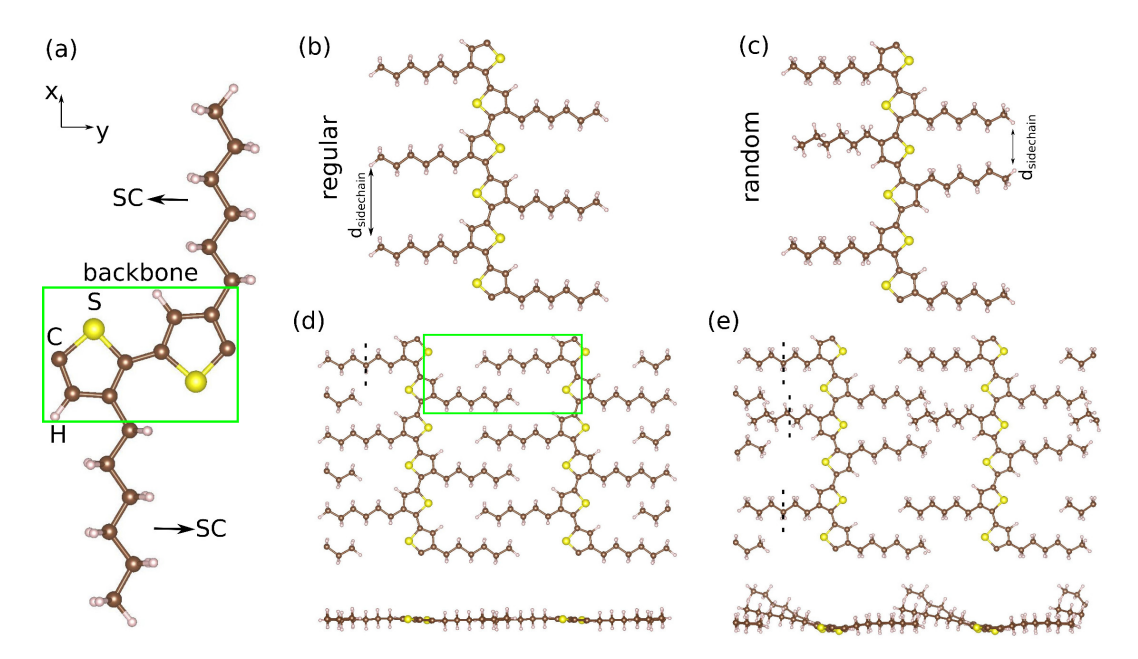


Figure 1: P3HT polymer in different conformations. (a) P3HT monomer, (b) regio-regular chain (ReP3HT), (c) regio-random chain (RaP3HT) (d-e) planar allotropes of ReP3HT and RaP3HT chains. In the ball-and-stick model C, S and H atoms are represented with brown, yellow and pink spheres, respectively.

regio-regular (ReP3HT) polymers where the side chains have the same orientation in each monomer and (ii) regio-random (RaP3HT) polymers where the side chains are attached to the backbone from random locations in alternating monomers. We note that, disordered and non-periodic structures can also form as a result of external factors in practical applications. In its ground state, the chain length in a period along the y-direction is 7.69Å which is in excellent agreement with previous experimental result of 7.7Å. In ReP3HT, the axes of the side chains remain perpendicular to the axis of the backbone during conjugate gradient geometry relaxation steps, whereas the side chains rotate in RaP3HT. Here we note that, there are various possible ways to construct a RaP3HT model (that can be obtained by attaching the side chains from different locations), and in Figure 1(c) we show only one of those arrangements. Another allotrope of P3HT, shown in Figure 1(d), is obtained by bringing individual periodic chains closer to each other on the same plane to create a thin layer of P3HT. In this geometry, the alkyl side chains of alternating P3HT units penetrate toward each other where the distance between the backbones of adjacent chains is 13.42Å.

Here it should be noted that as the chains are brought closer to each other, the ReP3HT structure preserves its initial planar geometry.

If we repeat a similar procedure to construct a thin layer of RaP3HT, the side chains rotate asymmetrically along backbone as shown in Figure 1(e). This is primarily due to the fact that the minimum distance between the side chains of adjacent polymers is lower in the RaP3HT as compared to the ReP3HT. These rotations induce further interaction between the side chains. In other words, while the C-C bond distances within a side chain of the ReP3HT are identical, the final stable structure of the RaP3HT have non-uniform bond length distribution in its side chains. For ReP3HT, the geometrical midpoint of each side chain aligns with its middle carbon atom (as indicated in the figure with dashed vertical lines). On the other hand, due to the attraction between adjacent polymers the side chains slightly stretch or shrink in the RaP3HT, and the geometrical center shifts away from the middle carbon atom. Hence, the uniformity of the material is distorted and the side chains of the RaP3HT rotate asymmetrically along backbone. Similarly, effects of geometrical asymmetry on the local magnetic states have been observed previously in atomic C and Si chain structures. ^{17–19}

As the side chains of RaP3HT rotate, the heads of adjacent chains get closer to each other and they create self-assembled disordered clusters. Since the charge transfer process in a given material is limited by the most difficult electron hopping process, which is often dominated by disordered regions, 6,13 the induced regio-randomness has important consequences on the electronic properties of P3HT. In Figure 2 we present the electronic structure of ReP3HT and the variation of band gap with increasing regio-randomness. Here, we quantify regio-randomness by measuring the minimum distance between side chains, $d_{sidechain}$, as indicated in Figure 1. Planar ReP3HT has a direct band gap of 1.1eV at the Γ point where the conduction band minimum (CBM) and valance band maximum (VBM) are mainly composed of the π_z states of the backbone. Upon performing Heyd-Scuseria-Ernzerhof (HSE) calculation on top of the GGA, the band gap at the Γ point increases to 1.6eV. The electronic

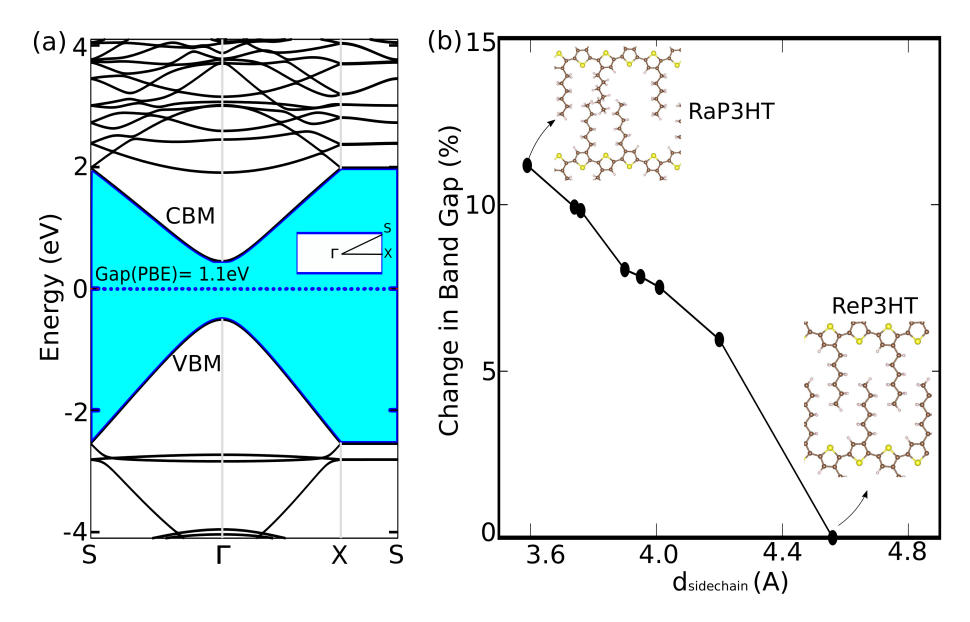


Figure 2: (a) Electronic band structure of planar ReP3HT. The inset shows the Brillouin Zone and the high symmetry points along which the band structure is calculated. The fundamental band gap at the Γ point increases to 1.6 eV after HSE calculation. (b) Variation of band gap at the Γ point as a function of the shortest distance between the sidechains $(d_{sidecahin})$ as illustrated in Figure 1. We note that the band gap always increases with $d_{sidecahin}$ and the perfect ReP3HT structure has the lowest band gap.

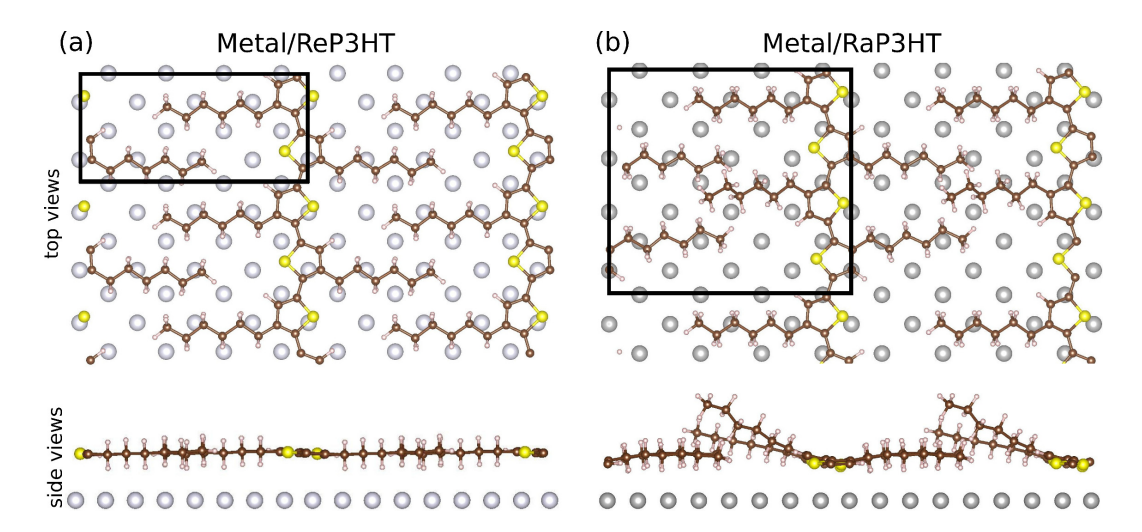


Figure 3: (a) Top and side views of the optimized geometries of (a) ReP3HT and (b) RaP3HT on metal substrate where only the atoms in the topmost metal layer is shown. The unit cells are indicated rectangles. The optimized in-plane lattice constants are 7.7 and 16.0 Å for ReP3HT and 15.7 and 16.9 Å for RaP3HT. The side views show the rotation of the side chains in the metal/RaP3HT system.

energy near the Γ -point of the BZ changes linearly with respect to $\mathbf{q}=\Gamma$ - \mathbf{k} , which leads to $E=\hbar v_F \mathbf{q}+O[(\mathbf{q}/\mathbf{k}^2])$ where v_F is the Fermi velocity. Therefore, by calculating the first derivative of the electronic energies of the π bands near the Γ -point with respect to \mathbf{q} , the Fermi velocity is calculated as $6.94\times 10^4 m/s$. Similarly, using the curvature of CBM around the Γ -point, the effective mass defined by $\hbar/m^*=1/(d^2E/dk^2)$, is calculated as $0.15m_e$ where m_e is the mass of an electron. Therefore, it is expected that there will be a high-mobility transport within the P3HT structure. As we start to introduce regio-randomness into the system, the band gap gradually increases as shown in Figure 2(b) where the band gap at the Γ -point is plotted as a function of the minimum distance between the side chains. The overall topology of the electronic band structure is conserved, but the band gap increases up to 11% in RaP3HT as compared to ReP3HT.

We next place the Re- and RaP3HT layers on metallic Au, Ag or Pt (001) surfaces to monitor the effect of regio-randomness on charge transfer at the interface. To reduce the computational cost in the current study, we model the metal/P3HT interfaces by using only one layer of P3HT where other P3HT layers can be grown on top of the first layer. In fact, previous studies have shown that the layer-layer distance of multilayer P3HT is large (3.8Å - 4.0Å) and metal - polymer interaction is dominated by the P3HT layer that is nearest to the metallic substrate. 16,20 To mimic the semi-infinite metal-polymer interaction, we use three layers of metallic sheets. As shown in Figure 3, the side chains of ReP3HT (RaP3HT) maintain their planar (rotated) orientations on the metallic substrate where the backbones are planar in both cases. For each case, the surface binding energy per unit cell is calculated from the expression $E_B = E_{P3HT} + E_{metal} - E_{[P3HT+metal]}$, in terms of the total energies of isolated P3HT, substrate and the combined metal/P3HT heterostructure where a positive value indicates adhesive binding. The binding energies between the substrates and the polymers per thiophene ring in the unit cells presented in Figure 3(a-b) were calculated as 2.92, 2.88, 2.11 eV for ReP3HT and 1.45, 1.43, 1.01 eV for RaP3HT on Ag, Au and Pt 001 surfaces, respectively. These values indicate that P3HT has a strong stability on the metal surfaces and the binding energies are comparable with those of similar structures which were reported in the literature as 1.42 eV for P3HT on ZnO surface and 2.17 eV for a single S-Au bond. ^{21,22} To investigate the effect of side chains on interfacial binding, we removed the side chains from ReP3HT and recalculated its binding energy on Au surface, which dropped from 2.88 eV to 1.53 eV. This shows that both the side chains and the backbone contribute significantly to the adhesion of P3HT polymer on the metal substrate, as also reported previously for the NiO/P3HT interface. ²¹ We note that, although the side chains do not perturb the backbone, they strengthen the surface binding energy between the metallic substrate and P3HT due to the increase in the contact area at the interface. This also explains the relatively lower binding energy of the RaP3HT polymer as compared to ReP3HT, since the side chains rotate away from the substrate in the metal/RaP3HT system which decreases interfacial contact area.

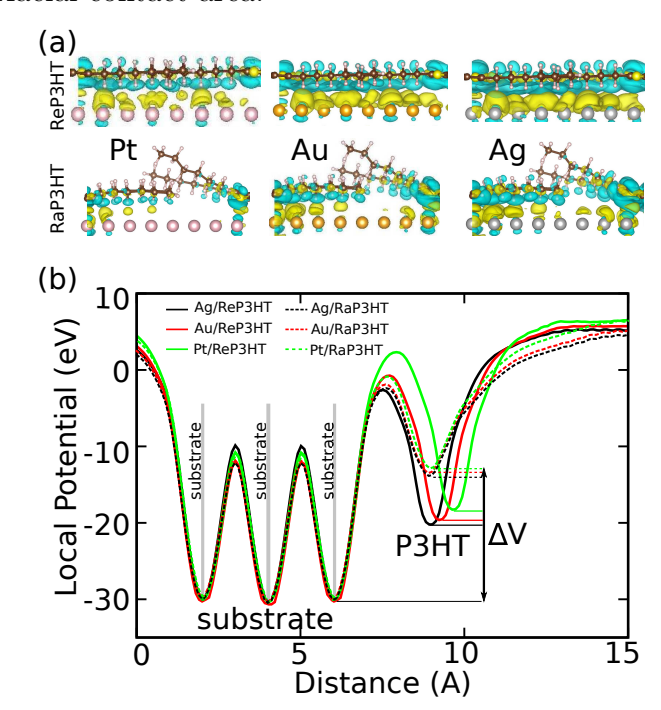


Figure 4: (a) Charge transfer isosurfaces for various metal/P3HT systems. Only the top layer of the substrate is shown. (b) Variation of the electrostatic local potential along the out-of-plane direction of the metal/P3HT systems shown in (a).

The charge distribution after the formation each metal/P3HT interface was obtained by calculating the difference of the local charge densities, $\Delta \rho$, of the heterostructure and individual materials using $\Delta \rho = \rho_{[metal+P3HT]} - \rho_{[P3HT]} - \rho_{[metal]}$ where each term of this equation is calculated separately in the same unit cell. The volumetric charge difference plots shown in Figure 4(a) were calculated using the same isosurface value for the sake of comparability. In each case, the substantial amount of electron-hole accumulation observed in the interlayer region indicates strong hybridization. Charge density populations per area on the surfaces were calculated as 0.061, 0.056, and 0.038 C/m² for Ag/ReP3HT, Au/ReP3HT and Pt/ReP3HT interfaces, respectively. These numbers drop to 0.051, 0.040, and 0.027 C/m² for Ag/RaP3HT, Au/RaP3HT and Pt/RaP3HT interfaces. The order of the surface charge density values in Ag, Au and Pt substrates follows the same trend as the binding energies of P3HT on these substrates, such that higher charge transfer leads to stronger The decrease in charge transfer after inducing regio-randomness to the P3HT polymer can also be seen in Figure 4(a). Our results show that both the side chains and the thiophene rings are contributing to spontaneous charge transfer between the metal substrate and P3HT. This is a similar behavior to the adhesive energy between P3HT and the metal surface as described above. Both the side chains and the thiophene rings are contributing to surface binding, which is related to spontaneous charge transfer.

The level of charge transfer at the interfaces also manifests itself in the distribution of the DFT computed local electrostatic potential difference as shown in Figure 4(b). Both for ReP3HT and RaP3HT, the difference between the potential of the metallic surface and the organic polymer is lower for the heterostructures with higher amount of charge transfer (namely, $\Delta V_{Ag-P3HT} < \Delta V_{Au-P3HT} < \Delta V_{Pt-P3HT}$). Replacing ReP3HT with RaP3HT also significantly increases the potential difference as shown by the dashed curves in Figure 4(b). Using the local electrostatic potential plots, the work functions of the interfaces were calculated by $\Phi_{workfunction} = E_{vacuum} - E_{Fermi}$ where E_{vacuum} is the vacuum potential which is equal to the value of the local potential in Figure 4(b) as $d \to \infty$ and E_{Fermi} is the energy of the highest occupied state of each system obtained from electronic structure calculations. The work functions of ReP3HT (RaP3HT) on Ag, Au, and Pt substrates are 3.43 (4.31),

4.19 (5.24) and 5.45 (6.98) eV, respectively. Here again, interfaces with more charge transfer have lower work functions, because as a result of electron transfer the energy gap between the Fermi level and the vacuum level is decreasing. In other words, the amount of work needed to remove an electron from the surface is decreasing. The work function of the isolated gold substrate was also calculated as 5.55 eV which indicates that the work function of the metal substrate can be engineered by depositing organic films to introduce charge transfers. It should be noted that, possible hydrocarbon/oxygen-based contamination²³ of the surfaces has been largely alleviated by routine Ozone cleaning under UV radiation, before preparing the P3HT/metal interfaces. Thus, such contamination will be neglegible both in the Regular and Random P3HT-metal heterostructures and the overall comparative trend presented here (which depends on the regio-randomness of the polymers) will not be effected by contamination. In addition to this, forming a P3HT / metal contact will cause a modification in the electron density of the clean surface and the dangling bonds leaking out from the metal surface will decrease the work functions reported here. A more realistic calculation might be investigating the contaminated surfaces computationally, however since contamination of the pure surfaces does not happen spontaneously in ground state DFT calculations, each contaminated surface should be manually created and recalculated at elevated temperatures.

The densities of electronic states are also affected by the charge transfer process at the interface as shown in Figure 5(a) for Au/ReP3HT and Au/RaP3HT. Accordingly, Au states fill the gap region of the isolated P3HT layer and the Fermi level of the system is just above the HOMO state of P3HT, which is set to zero in Figure 5(a). For example, in the heterostructure the first CBM state of ReP3HT (or RaP3HT) appears at 0.70 (or 0.85) eV, which is 0.40 (or 0.35) eV lower than the CBM energy of the freestanding ReP3HT (or RaP3HT). Thus, electron transfer from the P3HT layer to Au states is easily possible and it can lead to hybridization at the interface of the heterostructure. This is a direct indication of strong electronic coupling at the interface and high charge generation efficiency for photovoltaic applications where electrons can be pumped towards the conduction bands

upon exciton diffusion to the interface. We note that, although GGA underestimates the band gaps, we see that the band gap of P3HT decreases by $0.4~\rm eV$ after it is deposited on the gold substrate. This is consistent with experimental results, where we found that the initial band gap of ReP3HT is $2.1~\rm eV$ and by depositing ReP3HT on Au, we create an interfacial gap of $1.5~\rm eV$.

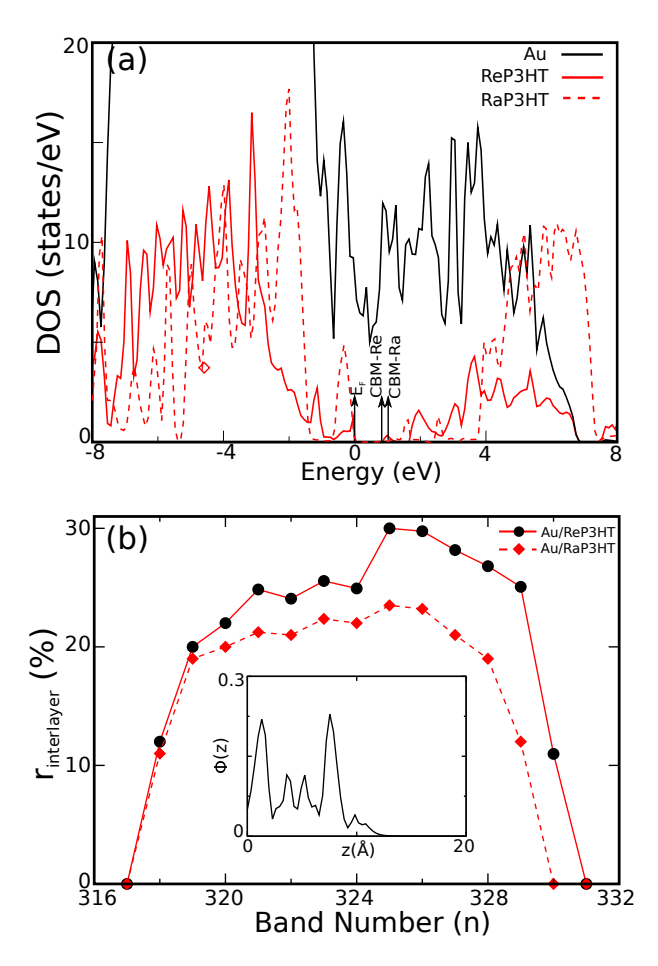


Figure 5: (a) Density of states projected onto P3HT and Au atoms in Au/ReP3HT and Au/RaP3HT. (b) Percentage of the interlayer states localized in the interlayer region of the Au/P3HT and Au/RaP3HT heterostructures on different bands are shown with black and red curves, respectively. The inset shows the probability density function, $\Phi(z)$, at the conduction band minimum of Au/ReP3HT.

We evaluate the level of hybridization by calculating the real space wavefunction along the material. Using the DFT calculated wave function data which includes the lattice points in the reciprocal space and their corresponding plane wave coefficients, real-space wavefunctions were constructed. Starting from the pseudo-wave function, $\Psi_{n,k}(r)$, of a specific band (n) at

a specified k-point, the probability function was extracted to a specified region in the real space as $\Phi(n) = \int_{z_1}^{z_2} dz \int_{\Omega} \Psi_{n,k}(r)^2 dxdy$, where Ω is the two-dimensional cross section of the unit cell, and z_1 - z_2 are the boundaries in the out-of-plane direction where the wavefunction is evaluated. Here, we focused on the wave function at the Γ point since that is where CBM and VBM of P3HT reside. We performed these calculations for different bands at the Γ point and calculate the percentage of states that are localized in the interlayer region as shown in Figure 5(b), where $r_{interlayer}$ is calculated by adding the probability functions in the interlayer region. Accordingly, ratio of states residing in the interface is higher in the Au/ReP3HT system as compared to Au/RaP3Ht where both heterostructures exhibit strong hybridization and interlayer coupling of electronic states. The decrease of $r_{interlayer}$ in Au/RaP3HT is consistent with its higher work function and lower level of charge transfer as compared to Au/ReP3HT.

Having shown the effect of regio-randomness on metal/P3HT interfaces, we finally compare the computational results with our experimental HD-VSFG data. HD-VSFG spectra measurements have been a sensitive tool for probing molecular structures at interfaces. ^{27–31} In principle, the top P3HT/air interface and bulk third order signal from P3HT could also contribute to the measured HD-VSFG signal. ^{9,29,32} Previously, ³³ we have conducted a thickness dependence VSFG measurement, and used this method to disentangle these three contributions. We concluded that the top interface and bulk contributions are negligible and it is the buried P3HT/metal interfaces dominating the HD-VSFG signal. This also agrees with intuitions, because it is only the electronic structure at the buried interfaces affected by creating the P3HT/metal heterojuction. Therefore only signal from this interface should be changed.

Here, we collect HD-VSFG spectra of different metal/P3HT systems using the spectrometer ^{10,33} that is schematically presented in Figure 6(a) and the results are shown in Figure 6(b). Accordingly, ReP3HT on all three metal substrates show significant amount of nonresonant signal where the Ag/P3HT system has the largest nonresonant signal followed by Au/P3HT

and Pt/P3HT. We note that since there is no SFG signal from bare metal films, all of the HD-VSFG data were taken under SSP polarization condition. There is no nonresonant signal by metal substrates themselves due to the large lateral screening of free electron motions. The fact that nonresonant signal becomes strong at metal/P3HT interfaces, indicates that there is a substantiate modification of the interfacial electronic structure. Furthermore, this nonresonant signal intensity trend agrees with the spontaneous charge transfer calculation shown in Figure 4(a) which suggests the origin of nonresonant signal is related to the charge redistribution across the interface. On the other hand, metal/RaP3HT systems have an overall smaller nonresonant signal, especially for Pt/RaP3HT where there is almost no nonresonant signal which further verifies the correlation between the spectral features to the electronic structure. The intensity of nonresonant signal show a linear correlation with the calculated spontaneous interfacial charge transfer as shown in the inset of Figure 6(b). There are two possible origins of the nonresonant signal in HD-VSFG spectra. First, the hybridization between the organic polymer and metal electronic orbitals significantly reduce the lateral screening force. Therefore, lateral free electron oscillation driven by the external electromagnetic field are not completely screened and SSP SFG signal becomes allowed. Second, interfacial charge transfer generates an interfacial electric field, which subsequently lead to a $\chi^{(3)}$ contribution of the nonresonant signal at interfaces. ³⁴ Further investigation will be necessary to completely explain the mechanism of spontaneous interfacial charge transfer induced nonresonant signal.

In conclusion, by combining ab-initio quantum chemical calculations based on DFT with HD-VSFG measurements, we showed that the geometrical conformation of the organic polymer at a metal/organic heterojunction is significant at determining the electronic properties of the system and the amount of charge transfer between the layers. Using simplified ReP3HT and RaP3HT model structures, we show that the electronic coupling at the interface and the work function of the material can be selectively engineered by modifying the level of regio-randomness present in the side chains of the P3HT polymer where increasing regio-

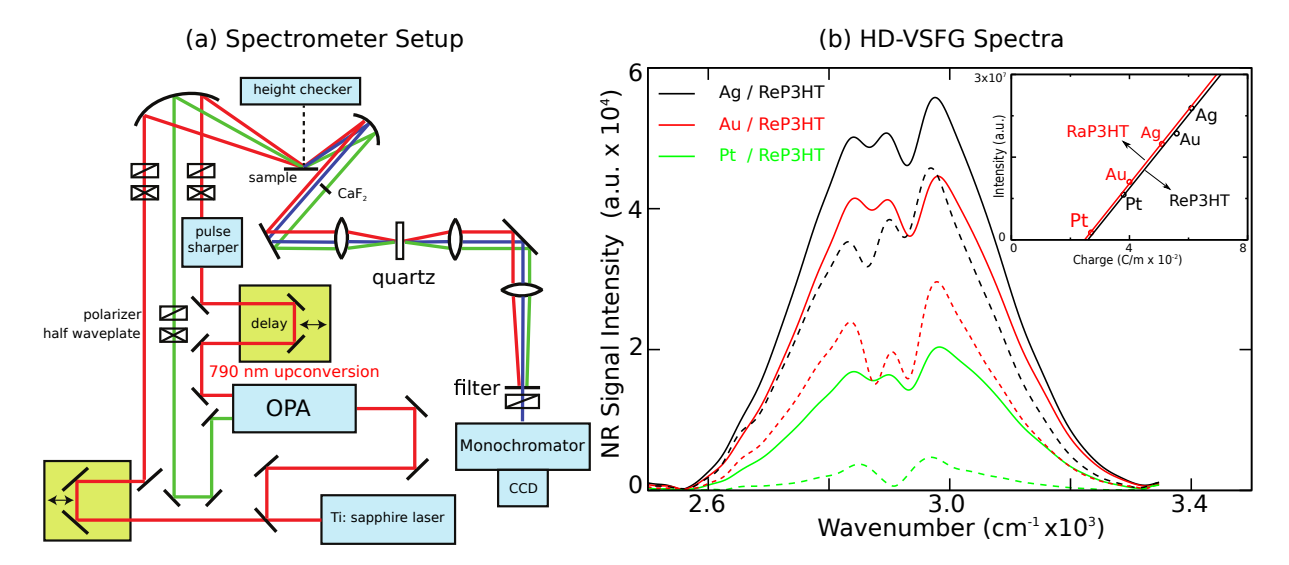


Figure 6: (a) Schematic description of the spectrometer that is used to collect the HD-VSFG spectra. (b) The nonresonant part of the HD-VSFG spectra of ReP3HT and RaP3HT polymers on different substrates are shown with solid and dashed curves, respectively. The inset shows the linear variation of the integrated nonresonant signal intensity with charge density at the interface.

randomness lowers the charge transfer and electronic coupling. We revealed that this effect is a direct consequence of the modification of the real space wave function of the material and hybridization of its electronic states. The theoretical predictions presented here are in agreement with our HD-VSFG measurements where both of which suggest that there is a direct correlation with the level of charge transfer and the intensity of the nonresonant response of the metal/P3HT systems. Thus, by measuring the non-resonant response of the metal/P3HT heterojunctions, we showed that there is strong correlation between the simulated charge transfer and measured non-resonant response. We finally note that, our results were obtained by using simplified models of RaP3HT polymers, which may not be exact representations of the actual samples used in the experiments. Further characterization experiments will be necessary to acquire the exact atomic configurations of the RaP3HT polymers deposited on metal substrates. However, by inducing regio-randomness into these simplified models, we were able to capture the effect of disorder on interfacial charge transfer that align with our HD-VSFG results. Thus, our results pave the way of a new theoretical and experimental approach for modeling probing the spontaneous charge transfer under

ambient condition.

Methods: First principles calculations were performed using the generalized gradient approximation including van der Waals corrections. ³⁵ Projector-augmented wave potentials ³⁶ were used and the exchange-correlation potential was approximated with the Perdew-Burke-Ernzerhof(PBE) functional.³⁷ The Brillouin zone(BZ) was sampled in the Monkhorst-Pack scheme where the **k**-point sampling of $(11\times11\times1)$ was found to be suitable for the BZ corresponding to the primitive unit cell of P3HT. For larger unit cells, the k-point sampling was scaled accordingly. Self-consistent field conjugate-gradient algorithm was used to relax the atoms into their ground states in periodic boundary conditions. While modeling the heterostructures, the size of the periodic unit cell in the out-of-plane direction was tested to be sufficiently large to avoid coupling between periodic units and a vacuum spacing of 10 Å was used. A plane-wave basis set with energy cutoff value of 450 eV was used where the energy convergence value between two consecutive steps was chosen as 10^{-5} eV. A maximum force of $0.1~{\rm eV/\AA}$ was allowed on each atom. The electronic band structures were calculated using the pre-converged unit cells and charge distributions. The band structures were calculated along the $S-\Gamma-X-S$ high symmetry points in the first BZ where 50 **k**-points were used between each high symmetry point. The band gaps were obtained from the difference of conduction band minimum and valance band maximum energies in the band structures. Numerical calculations were carried out using the VASP software. 38 It is known that ground state PBE calculations underestimate the fundamental band gap of heterostructure systems. Here, to evaluate the effect of using PBE and to increase accuracy of our results, for the Au/ReP3HT structure, we also performed calculations using the HSE06 hybrid functional, ³⁹ which is constructed by mixing 25% of the Fock exchange with 75% of the PBE exchange and 100% of the PBE correlation energy. As expected, the result showed that PBE underestimates the band gap (by 30%). We note that, the unit cell of each heterostructure presented in this paper contains more than 200 atoms. Since computing the full electronic structure of the heterostructures using HSE would be computationally very costly, and the overall character of the electronic structure would be similar to those obtained by PBE calculations, here we only present results based on PBE. We also not that, although our computational treatment ignores the molecular nature of the polymer, the polymer is strongly coupled to the solid metallic substrate. The heterostructure material (with includes the periodic polymer layer) acts together with the metal as a solid state system. Therefore using solid-state methods is realistic for capturing the electronic properties of the heterostructure.

The metal/P3HT interfaces used in HD-VSFG experiments were prepared by spin coating method at 1500 rpm. Regioregular (REIKE Metal) and regiorandom P3HT (Sigma Aldrich) were dissolved in chloroform with the concentration of 8 mg/ml respectively. The metal substrates were prepared by magnetron sputtering where a titanium layer was firstly sputtered onto glass slice to improve the adhesion between metals and glass substrates, followed by depositing gold, silver, and platinum on top where the thickness is determined to be 150 nm. For the HD-VSFG experiments, the light source is an ultrafast Ti:sapphire regenerative amplifier (Astrella, Coherent) that outputs 790 nm pulses with 5W power. The 790 nm beam is then sent into an optical parametric amplifier (TOPAS, Light Conversion) to generate two tunable near-IR pulses which are referred as signal and idler beam. The two near-IR beams are then spatially and temporally overlapped on a type I BBO crystal to generate the mid-IR beam that centers at 3.3 μ m to be on resonant with the C-H vibrational mode in P3HT. The residual 790 nm beam after TOPAS is used as upconversion beam which passes through a spectral pulse shaper to narrow down the spectral bandwidth to 0.6 nm or 9.5 cm-1 at full-width half max (FWHM) to improve the spectral resolution. The HD-VSFG signal is generated by spatially and temporally overlapping the mid-IR pulse and upconversion pulse at the sample surface. The reflected mid-IR pulse then passes through a 2-mm thick CaF2 delay media to generate a time delay relative to the HD-VSFG signal. The upconversion beam and delayed mid-IR beam are then focused onto a Y-cut quartz crystal by a lens (f=10 cm) to generate the local oscillator (LO) for heterodyne detection. Both LO and HD-VSFG signals are collimated by another lens (f=10 cm) and then transmit through a short-band pass filter to remove the 790 nm residual. After passing through the monochromator, the LO and HD-VSFG signals interfere with each other at a charge-coupled device (CCD) to generate the heterodyne HD-VSFG signal.

Acknowledgments: This research was supported by the National Science Foundation (NSF) through grant CHE-1808111. All computations were performed using the resources of the Extreme Science and Engineering Discovery Environment (XSEDE), which is supported by the NSF through grant ACI-1053575, under allocation TG-CHE110009.

References

- (1) Bae, S.-H.; Kum, H.; Kong, W.; Kim, Y.; Choi, C.; Lee, B.; Lin, P.; Park, Y.; Kim, J. Integration of Bulk Materials with Two-Dimensional Materials for Physical Coupling and Applications. *Nat. Mater.* **2019**, *18*, 550.
- (2) Huynh, W. U.; Dittmer, J. J.; Alivisatos, A. P. Hybrid Nanorod-Polymer Solar Cells. Science 2002, 295, 2425–2427.
- (3) Yin, Y.; Alivisatos, A. P. Colloidal Nanocrystal Synthesis and the Organic–Inorganic Interface. *Nature* **2004**, *437*, 664.
- (4) Coakley, K. M.; McGehee, M. D. Conjugated Polymer Photovoltaic cCells. *Chem. Mater.* **2004**, *16*, 4533–4542.
- (5) Chang, J. A.; Rhee, J. H.; Im, S. H.; Lee, Y. H.; Kim, H.-j.; Seok, S. I.; Nazeerud-din, M. K.; Gratzel, M. High-Performance Nanostructured Inorganic-Organic Hetero-junction Solar Cells. *Nano Lett.* 2010, 10, 2609–2612.
- (6) Braun, S.; Salaneck, W. R.; Fahlman, M. Energy-Level Alignment at Organic/Metal and Organic/Organic Interfaces. *Adv. Mater.* **2009**, *21*, 1450–1472.

- (7) Dag, S.; Wang, L.-W. Modeling of Nanoscale Morphology of Regionegular Poly(3-Hexylthiophene) on a ZnO (1010) Surface. *Nano Lett.* **2008**, *8*, 4185–4190.
- (8) Dag, S.; Wang, L.-W. Packing Structure of Poly(3-Hexylthiophene) Crystal: Ab initio and Molecular Dynamics Studies. *J. Phys. Chem. C* **2010**, *114*, 5997–6000.
- (9) Anglin, T. C.; O'Brien, D. B.; Massari, A. M. Monitoring the Charge Accumulation Process in Polymeric Field-Effect Transistors via in Situ Sum Frequency Generation. J. Phys. Chem. C 2010, 114, 17629–17637.
- (10) Xiang, B.; Li, Y.; Pham, C. H.; Paesani, F.; Xiong, W. Ultrafast Direct Electron Transfer at Organic Semiconductor and Metal Interfaces. *Sci. Adv.* **2017**, *3*, e1701508.
- (11) Lindau, I.; Spicer, W. The Probing Depth in Photoemission and Auger-Electron Spectroscopy. J. Electron. Spectrosc. Relat. Phenom 1974, 3, 409–413.
- (12) Wang, G.; Moses, D.; Heeger, A. J.; Zhang, H.-M.; Narasimhan, M.; Demaray, R. Poly(3-Hexylthiophene) Field-Effect Transistors with High Dielectric Constant Gate Insulator. J. Appl. Phys. 2004, 95, 316–322.
- (13) Sirringhaus, H.; Brown, P.; Friend, R.; Nielsen, M. M.; Bechgaard, K.; Langeveld-Voss, B.; Spiering, A.; Janssen, R. A.; Meijer, E.; Herwig, P.; Leeuw, D. M. Two-Dimensional Charge Transport in Self-Organized, High-Mobility Conjugated Polymers.

 Nature 1999, 401, 685.
- (14) Dang, M. T.; Hirsch, L.; Wantz, G. P3HT: PCBM, Best Seller in Polymer Photovoltaic Research. Adv. Mater. 2011, 23, 3597–3602.
- (15) Holliday, S.; Ashraf, R. S.; Wadsworth, A.; Baran, D.; Yousaf, S. A.; Nielsen, C. B.; Tan, C.-H.; Dimitrov, S. D.; Shang, Z.; et. al., High-Efficiency and Air-Stable P3HT-Based Polymer Solar Cells with a New Non-Fullerene Acceptor. *Nat. Commun.* 2016, 7, 11585.

- (16) Sirringhaus, H.; Brown, P.; Friend, R.; Nielsen, M. M.; Bechgaard, K.; Langeveld-Voss, B.; Spiering, A.; Janssen, R.; Meijer, E. Microstructure–Mobility Correlation in Self-Organised, Conjugated Polymer Field-Effect Transistors. Synth. Met. 2000, 111, 129–132.
- (17) Fan, X.; Liu, L.; Lin, J.; Shen, Z.; Kuo, J.-L. Density Functional Theory Study of Finite Carbon Chains. *ACS Nano* **2009**, *3*, 3788–3794.
- (18) Cahangirov, S.; Topsakal, M.; Ciraci, S. Long-Range Interactions in Carbon Atomic Chains. *Phys. Rev. B* **2010**, *82*, 195444.
- (19) Özçelik, V. O.; Ciraci, S. Self-Assembly Mechanisms of Short Atomic Chains on Single-Layer Graphene and Boron Nitride. *Phys. Rev. B* **2012**, *86*, 155421.
- (20) Brinkmann, M.; Wittmann, J.-C. Orientation of Regioregular Poly(3-Hexylthiophene) by Directional Solidification: A Simple Method to Reveal the Semicrystalline Structure of a Conjugated Polymer. *Adv. Mater.* **2006**, *18*, 860–863.
- (21) Li, L.-H.; Kontsevoi, O. Y.; Freeman, A. J. Atomic-Scale Understanding of the Interaction of Poly(3-Hexylthiophene) with the NiO (100) Surface: A First-Principles Study. J. Phys. Chem. C 2014, 118, 20298–20305.
- (22) Pensa, E.; Cortes, E.; Corthey, G.; Carro, P.; Vericat, C.; Fonticelli, M. H.; Benitez, G.; Rubert, A. A.; Salvarezza, R. C. The Chemistry of the Sulfur–Gold Interface: In Search of a Unified Model. Acc. Chem. Res. 2012, 45, 1183–1192.
- (23) Crispin, X.; Geskin, V.; Crispin, A.; Cornil, J.; Lazzaroni, R.; Salaneck, W. R.; Bredas, J.-L. Characterization of the Interface Dipole at Organic/Metal Interfaces. J. Am. Chem. Soc 2002, 124, 8131–8141.
- (24) Feenstra, R. M.; Srivastava, N.; Gao, Q.; Widom, M.; Diaconescu, B.; Ohta, T.; Kel-

- logg, G.; Robinson, J.; Vlassiouk, I. Low-Energy Electron Reflectivity from Graphene. *Phys. Rev. B* **2013**, *87*, 041406.
- (25) Özçelik, V. O.; Fathi, M.; Azadani, J. G.; Low, T. Tin Monochalcogenide Heterostructures as Mechanically Rigid Infrared Band Gap Semiconductors. *Phys. Rev. Mater.* **2018**, 2, 051003.
- (26) Chaves, A.; Azadani, J.; Özçelik, V. O.; Grassi, R.; Low, T. Electrical Control of Excitons in van der Waals Heterostructures with Type-II Band Alignment. *Phys. Rev.* B 2018, 98, 121302.
- (27) Zhuang, X.; Miranda, P.; Kim, D.; Shen, Y. Mapping Molecular Orientation and Conformation at Interfaces by Surface Nonlinear Optics. *Phys. Rev. B* **1999**, *59*, 12632.
- (28) Hore, D. K.; Beaman, D. K.; Parks, D. H.; Richmond, G. L. Whole-Molecule Approach for Determining Orientation at Isotropic Surfaces by Nonlinear Vibrational Spectroscopy. J. Phys. Chem. B 2005, 109, 16846–16851.
- (29) O'Brien, D. B.; Massari, A. M. Experimental Evidence for an Optical Interference Model for Vibrational Sum Frequency Generation on Multilayer Organic Thin Film Systems. Consideration for Higher Order Terms. J. Chem. Phys. 2015, 142, 024704.
- (30) Wang, H.-F.; Velarde, L.; Gan, W.; Fu, L. Quantitative Sum-Frequency Generation Vibrational Spectroscopy of Molecular Surfaces and Interfaces: Lineshape, Polarization, and Orientation. *Annu. Rev. Phys. Chem.* **2015**, *66*, 189–216.
- (31) Li, Y.; Wang, J.; Xiong, W. Probing Electronic Structures of Organic Semiconductors at Buried Interfaces by Electronic Sum Frequency Generation Spectroscopy. J. Phys. Chem. C 2015, 119, 28083–28089.
- (32) Pandey, R.; Moon, A. P.; Bender, J. A.; Roberts, S. T. Extracting the Density of

- States of Copper Phthalocyanine at the SiO₂ Interface with Electronic Sum Frequency Generation. J. Phys. Chem. Lett. **2016**, 7, 1060–1066.
- (33) Li, Y.; Xiang, B.; Xiong, W. Heterodyne Transient Vibrational SFG to Reveal Molecular Responses to Interfacial Charge Transfer. J. Chem. Phys. **2019**, 150, 114706.
- (34) Ohno, P. E.; Wang, H.-f.; Geiger, F. M. Second-Order Spectral Lineshapes from Charged Interfaces. *Nat. Commun.* **2017**, *8*, 1032.
- (35) Grimme, S. Semiempirical GGA-type Density Functional Constructed with a Long-Range Dispersion Correction. *J. Comput. Chem.* **2006**, *27*, 1787–1799.
- (36) Blöchl, P. E. Projector Augmented-Wave Method. *Phys. Rev. B* **1994**, *50*, 17953–17979.
- (37) Perdew, J. P.; Burke, K.; Ernzerhof, M. Generalized Gradient Approximation Made Simple. *Phys. Rev. Lett.* **1996**, *77*, 3865–3868.
- (38) Kresse, G.; Furthmüller, J. Efficient Iterative Schemes for Ab Initio Total-Energy Calculations Using a Plane-Wave Basis Set. *Phys. Rev. B* **1996**, *54*, 11169–11186.
- (39) Paier, J.; Marsman, M.; Hummer, K.; Kresse, G.; Gerber, I. C.; Ángyán, J. G. Screened Hybrid Density Functionals Applied to Solids. *J. Chem. Phys.* **2006**, *124*, 154709.

TOC Figure

